Rapid prototyping of geosynthetic interfaces: Investigation of peak strength using direct shear tests

Rapid Prototyping of Geosynthetic Interfaces: Investigation of Peak Strength Using Direct Shear Tests

Gary John Fowmes[1], Neil Dixon[2], Liwei Fu[3] and Catalin Alexandru Zaharescu[2]

1. Corresponding author, School of Engineering, University of Warwick, CV4 7AL, UK. Tel: +44(0)2476 5 28006. G.Fowmes@Warwick.ac.uk

2. School of Civil and Building Engineering, Loughborough University, Loughborough, LE11 3TU, UK. N.Dixon@lboro.ac.uk; C.A.Zaharescu@lboro.ac.uk

3. Advanced Laser Technology Ltd. 9, Piccadilly Trading Estate in Manchester, M1 2NP, UK. liweifu@outlook.com,

Text: 5680 Words; 5 Tables; 14 Figures

Abstract

Rapid prototyping offers a platform technology for investigations within the geosynthetics research and manufacturing sectors. This paper considers the application of rapid prototyping for the development of geosynthetic interfaces. The benefits and challenges of three rapid prototyping techniques (fused filament fabrication, selective laser sintering and laser thermal ablation) are considered and comparisons are presented between the three technologies. The paper then compares prototyped models of geomembrane texturing to those of a factory sourced reference geomembrane, leading on to a systematic geometric assessment using laser sintered model geomembranes. The geometric assessment highlights the benefits of hooked geomembrane asperities to interact with geotextiles in low normal stress applications, with a 69% increase in peak shear strength reported for hooked asperities, compared to the factory reference geometry. Asperity spacing is shown to influence the measured shear strength, with an increase for a geomembrane geotextile interfaces with closer asperities and an optimum spacing observed for geomembrane clay interfaces, below which the failure plane slides over the top of the texturing. Increases in asperity height correlated to smaller than expected increases in shear stresses for both geomembrane-geotextile and geomembrane clay interfaces.

Whilst current rapid manufacturing techniques are shown to offer the ability to test the influence of variables on the performance characteristics of geosynthetic materials, the limitations of each technique, polymer utilised and resulting chemical and physical behaviour of the sample must be understood to allow these techniques to be successfully deployed.

Key words: Geosynthetics, Geomembrane Texturing, Interfaces, Additive Manufacture, 3D printing, Rapid Prototyping.

1 Introduction

Construction using geosynthetics offer savings both in terms of cost and embodied carbon. However, geosynthetics interfaces are possible planes of weakness and have the potential to cause failure of geotechnical structures. Failures in landfills involving interfaces have been historically reported (e.g. Bergado et al., 2006; Koerner and Soong, 2000; Filz et al., 2001; Jones and Dixon, 2003) and these interfaces are of increasing importance with higher, steeper slopes required in mining applications (Lupo, 2010). Higher strength and more reliant interaction between geosynthetics and adjacent materials will allow steeper, higher and safer slopes to be constructed. Moreover, with an increasing emphasis on sustainable infrastructure, increased geosynthetic interface performance will allow more widespread application of these materials in construction applications, including uses with marginal fill materials (e.g. fine grained soils).

This paper focuses on the use of 3D printing to develop better understanding of interfaces involving geomembranes. These materials are continuous polymeric sheets formed by extruding of the polymer with either smooth or textured surfaces. The texturing can be formed by several methods, typically these include;

- Coextrusion (a secondary extruder adds a molten resin which contains a blowing agent to form the texturing;
- Lamination (where a foaming agent together with additional polymer is laminated to a smooth geomembrane);
- Impingement (where additional hot polymer is sprayed onto the surface); or
- Structured texturing (where a structured pattern is pressed into the molten geomembrane).

The development of peak strength occurs as the result of a mechanical interaction. Several studies have proposed differing methods of interlock from hook and loop interactions for geomembrane-geotextile interfaces (Hebeler et al., 2005) to the ploughing effect of sand on a coarse soil-geomembrane interface (Dove & Frost, 1999; Zettler, et al., 2000). If higher strength interaction between geosynthetics and adjacent materials can be achieved, this will allow steeper, higher and safer slopes to be constructed, thus facilitating sustainable construction using geosynthetic materials. Within any of the texturing techniques, manufacturers can alter the height, shape and frequency of the asperities on the textured surface. However, structured texturing allows greater design of textures rather than more random manufacturing driven texture

63 configurations (e.g. produced by coextrusion technique). Patterned rollers can be changed independently on
64 either side of the sheet while the rest of the manufacturing process remains the same. There are several
65 proprietary geomembrane surface textures available, but there is a dearth of scientific literature on what
66 characteristics of the texturing are responsible for generating strength, and hence a lack of guidance on which
67 characteristics can be combined and enhanced to give significant strength increases at geosynthetic interfaces.

68 A wealth of literature is available for the interface between geomembranes and geotextiles, fine grains soils
69 and coarse grained soils including some large databases of results (e.g. Dixon et al., 2006; Koerner and Narejo,
70 2005; McCartney et al., 2009; Triplett and Fox, 2001; Sia and Dixon, 2007), however, whilst some studies have
71 considered comparison between texturing types and quantification of surface roughness (Dove and Frost,
72 1996; Vangla and Latha, 2016) previous scientific investigation of the influence of geometric variables has been
73 difficult to achieve as systematically altering a variable in production is onerous. Numerical analyses, such as
74 those by Jing e*t al.* (2017) offer a possibility of investigating shape and spatial variability at interfaces,
75 however, such analyses require physical validation. This study considers the use of rapid manufacturing
76 techniques in the prototyping of geosynthetic interfaces, allowing the scientific evaluation of the key variables
77 controlling interface behaviour.

78 Recent developments in rapid manufacturing techniques offer the geosynthetic industry the potential for
79 prototyping and manufacture of products. Fowmes *et al.* (2016) carried out preliminary studies on 3D printed
80 interfaces and Stathas *et al*. (2017) used 3D Printing to create model geogrids, however, there remain
81 significant challenges for the use of such technologies as the polymeric materials typically adopted in
82 geosynthetic materials are not the same as those commonly used for polymeric printing processes. The paper
83 considers the benefits and challenges of rapid manufacturing techniques and presents comparisons between
84 technologies. The paper then compares prototyped models of texturing to those of a factory reference
85 geomembrane, leading on to a systematic geometric assessment using laser sintered model geomembranes.

86 **2 Rapid Prototyping Techniques**

87 Three prototyping techniques were trialled; two additive manufacturing, whereby material is built up in layers
88 using fusion or sintering techniques, and a subtractive method, whereby material was systematically removed
89 using a laser. It should be noted that other techniques exist and this is not intended to be an exhaustive list of

all potential prototyping techniques. This section provides details of the most applicable of the currently readily available techniques that have been trialled and discusses the challenges faced with each in the production of prototypes suitable for scientific investigations.

2.1 Additive manufacture: Fused Filament Fabrication

Fused Filament Fabrication (FFF), which is often used synonymously with 3D printing, involves the extrusion of molten polymeric filament such that the printed structure is built up in layers. The technique utilises cheap and readily available equipment, thus allowing rapid take up of the technology by researchers and manufacturers. However, the layer by layer build up results in heterogeneous strength and the likelihood of delamination between layers (Fowmes *et al.* 2016). This problem is further exacerbated when using textured geomembranes as the texturing is easily removed from the sheet along the internal structural laminations requiring the use of inclined or vertical build orientations (Figure 1). FFF typically utilises Polylactic Acid (PLA) or Acrylonitrile Butadiene Styrene (ABS), with the latter requiring higher print temperatures and having a greater tendency to shrink on cooling. Whilst ideally model geomembranes would utilise High Density Polyethylene (HDPE) and Polypropylene (PP), the authors' experience along with published literature (e.g. Baechler et al., 2013) show these materials are problematic to print due to their thermal, rheological and chemical properties leading to them having a tendency to deform, peel and delaminate. Thus, there is a dichotomy between the materials used for geosynthetics and those typically adopted for 3D printing applications (Fowmes et al. 2016). Where FFF is described in this paper, a PLA spool was utilised, thus representing a readily available and commercially accessible prototyping option. For the samples produced for this investigation a Flashforge Finder FFF printer was used with a print resolution of 0.10 mm, layer thickness of 0.10mm at a positional accuracy of ±0.002mm.

2.2 Additive manufacture: Selective Laser Sintering

Selective Laser Sintering (SLS) was chosen as one of the prototyping methods for this research project as a large quantity of samples can be produced with very high dimensional accuracy all in one process. SLS is a process that solidifies successive layers of powder material on top of each other, allowing the formation of complex 3D objects; achieved by heating up selective parts of the powder to its sintering temperature with a laser beam (Kruth, 1991). Sintering of the powder occurs as the grain viscosity drops with temperature; thereby, causing the surface tensions to be overcome and creating an artificial knitting of the grains without

full melting (Kruth, 1991). Scanning mirrors control the process, ensuring the laser beam scans each layer according to the corresponding cross section in a CAD or stereo-lithography file (Kruth, et al., 2003; Goodridge, et al., 2012). The powder supply system deposits thin layers of the powder in a building container before that layer is sintered and the process repeats itself until the entire object has been constructed. The powder that has not been sintered in each layer remains in place to support the next layer of powder or possible overhangs of the product and is removed, in this case with compressed air, on completion of the sintering process to reveal the final 3D object (Kruth, et al., 2003).

SLS has the ability to produce products with a wide range of materials. These materials include polycarbonate (PC), nylon, wax, ceramic and metal-polymer powders (Gibson & Shi, 1997). The most widely applied material in SLS and the most popular two used are amorphous polycarbonate (PC) and semi-crystalline polyamide (PA) (Schmid, et al., 2014). While amorphous polymers produce parts with good accuracy, resolution and surface finish, they are only partially consolidated, therefore, are not suitable where strength and durability are key properties required (Kruth, et al., 2003). Semi-crystalline polymers such as PA, on the other hand, can be sintered to fully dense parts that make them suited to prototypes where high strength is required (Gibson & Shi, 1997; Kruth, et al., 2003). One concern of using PA polymers is that shrinkage of the grains during sintering can cause build accuracy and surface finish to be compromised (Kruth, et al., 2003), however, the development of new grades of nylon powders in recent years has minimised this and led to the success of polyamide 12 (PA12) as the most common currently used in the SLS process (Schmid, et al., 2014).

In order to be effective in the SLS process, a polymer must fulfil certain fundamental properties. Schmid et al. (2014) categorises these properties into powder and particle; extrinsic that can be controlled by production, and thermal, optical and rheological molecular behaviour; intrinsic that cannot be easily influenced. The powder itself has to have an appropriate particle size distribution (PSD) to be effective, preferably between 20-80µm, and contain a low proportion of small particles, which induce greater adhesion and reduce flow of the powder (Schmid, et al., 2014). Secondly, the particles used should be rounded in nature to further enhance the free-flowing behaviour of the powder. This will achieve better powder density, therefore, better density of the final build (Schmid, et al., 2014). In terms of intrinsic molecular behaviour, the thermal properties are extremely important because the polymer must have a sufficient sintering window between melting and crystallisation so that it can be held within this temperature range whilst several layers are sintered in order to

provide good adhesion of the particles to previous layers (Schmid, et al., 2014). The melting temperature of PA12 is often in the region of around 175°C (Jollivet, et al., 2009) so the powder is heated to just below this temperature to ensure no melting of the particles occurs while crystallisation does. Optical properties are required to allow the powder to absorb energy at the laser wave length, however, an increase in laser power can compensate for poor absorption meaning this is less critical in choosing a polymer (Schmid, et al., 2014). Finally, rheological properties are critical as low viscosity and surface tension are required to generate sufficient coalescence of the polymer particles (Schmid, et al., 2014). Clearly these fundamental properties play a vital role in determining the mechanical properties of the finished build and should be considered carefully when attempting to prototype geosynthetics using the SLS method. The slice thickness is the depth which the powder bed lowers for each layer, and usually has a lower bound of around 0.07mm (Gibson & Shi, 1997). Small slice thickness reduces surface roughness, increases the dimensional accuracy of the build, but will increase the build time (Goodridge, et al., 2012).

As with FFF, the build orientation should also be carefully considered due to the anisotropic nature of SLS materials, in particular PA12 (Goodridge, et al., 2012; Fowmes et al., 2016). This anisotropic behaviour can be explained by the layer-layer build process of laser sintering. One way of countering this effect is to build the part with small cross sections, which will retain heat better and form stronger bonds with the next layer (Gibson & Shi, 1997; Goodridge, et al., 2012), however, this can lead to warping if large but thin parts are built upright (Goodridge, et al., 2012). For the samples produced for this investigation an EOS Formiga P100 system 24 was used to build the prototypes. This system used a recoating blade to pull the powder across the build area and a thin slice thickness was implemented to allow good dimensional accuracy of the final build. The machine has a radiant heater above and two convector heaters beside the build chamber to control the temperature of the powder; important because uneven cooling of the build can lead to problems when trying to achieve reproducible mechanical properties of prototypes (Goodridge, et al., 2012). The raw material from which the powder was formed is PA2200 (polyamide) due to its suitability in the EOS Formiga P100 system and its ability to achieve a quality finish and to withstand high mechanical loads. The PA2200 has an average grain size of 56μm and the potato shaped nature of the particles induces flow of the powder, making the sintering process more effective. The samples were built in vertical orientation to avoid the risk of lamination occurring between layers during the shear tests.

174 **2.3 Subtractive Manufacture**

175 In subtractive manufacture, a thicker initial sheet is used and material is removed to create the required
176 surfaces (see Figure 2). Several potentially subtractive manufacturing techniques are available, including CNC
177 milling, high pressure hydraulic cutters, and Laser Thermal Ablation (LTA). LTA was selected in this trial as it
178 employs a low powered laser allowing material to be cut without removing the full sheet thickness. In a LTA
179 process, unwanted material is eliminated through the photothermal ablation effect. A 3mm thick
180 geomembrane was used as the starting material, and patterns were "carved" by a 10.6μm CO_2 laser with X-Y
181 control. The ablated area was thermally removed by a moving laser beam, leaving a 3D surface pattern with
182 structure height at around 1mm on a 2 mm thick base sheet.

183 Subtractive manufacturing has inherent advantages in creating replicas of geomembranes used in industry as
184 the starting point uses the same, albeit thicker, geomembrane material with the same manufacturing method
185 and has no potential for delamination of the texturing that exists when using additive manufacturing methods
186 due to the layering of material. However, disadvantages with the laser equipment were, slow prototyping time
187 and the limited dimensional accuracy of this technique compared to SLS techniques. The authors were unable
188 to satisfactorily recreate the texting on the reference factory geomembrane, therefore, only additive
189 manufacturing methods were taken forward for trials within this reported study.

190 **3 Programme of testing**

191 A series of direct shear tests were carried out using either factory HDPE geomembrane or additive
192 manufactured prototypes sheared against either i) needle-punched non-woven geotextile, ii) Leighton Buzzard
193 Sand (LBS) or iii) Mercia Mudstone (MM).

194 A non-woven needle punched geotextile, typically used as a protection layer, was used throughout this batch
195 of tests. The material was sourced from the single roll, avoiding the end 3m of the roll. The properties of the
196 geotextile are given in Table 1. The reference geomembrane was a flat die extruded 1.5 mm thick HDPE
197 material with structured texturing. The properties of the geomembrane are presented in Table 2.

198 For the Geomembrane-Sand tests a uniformly graded (with 87% between 1 and 2mm) sand was used. Material
199 from the same batch was utilised throughout the test and to further maintain consistency. Sand was poured

200 into the shearbox and levelled with a straight edge. No compaction was carried out upon introduction into the
201 shear box, giving a density of 16.9 kN/m^3.

202 Mercia Mudstone (MM) was selected as the fine grained soil for testing as this is representative of typical
203 landfill liner materials in the UK. The properties of the MM are presented in Table 3. The material was mixed
204 from dry powder in a blade mixer to 17.0% (±0.3%) moisture content prior to testing. The material was batch
205 prepared and moisture content checked prior to placement in the shear apparatus. Compaction was carried
206 out at 17% moisture content (plastic limit) to achieve 95% maximum dry density.

207 A small direct shear apparatus was used in this case (100 x 100mm) modified for geosynthetics testing with a
208 constant shear area, the smaller device being preferred in this study due to the larger number of test
209 permutations that could be produced via the prototyping methods. The DSA used for the 100x100mm samples
210 was limited to 19mm of displacement, therefore, only peak strengths are compared. Whilst it is acknowledged
211 that many common interfaces exhibit strain softening behaviour (Thiel 2001; Koerner and Bowman, 2003),
212 improvements in peak strength are sought by designers and manufacturers, and interface resilience (i.e.
213 resistance to post peak loss) will be the topic of further investigation.

214 A shearing rate of 1mm/min was adopted for the tests with 1 hour of pre-compression prior to test
215 commencing. For the soil samples, measurements of vertical displacement were made throughout the pre-
216 consolidation phase. In trials, 90% of vertical displacement was achieved within one hour, therefore, to
217 facilitate the large number of tests, and to reduce the likelihood of moisture content changes at the sample
218 boundaries, a value of 1 hour was selected. Whilst for geomembrane-geotextile and geomembrane-sand
219 interfaces the strain rate will not significantly affect results compared to a slower rate (Tan et al., 1998; Godley
220 et al., 2015; Stark et al., 1996), geomembrane clay interfaces are rate sensitive due to the drainage state of the
221 interfaces. At 1mm/minute it is assumed that this resulted in predominantly undrained, repeatable, stress
222 conditions. Tests were carried out unsubmerged. The primary intention of the test method selected is to allow
223 comparison between samples rather than to represent a specific set of field conditions and adopting a
224 repeated method achieves this.

225 During the parametric investigation a number of asperity types have been applied. Firstly, a conical “spike”, as
226 used in the factory reference geomembrane, a “hook” asperity, which is a conical asperity with an angled

upper portion, and a “rib” which is a continuous flat sided asperity (see Figure 3). The rib design has been adopted in this experiment based on the knurled plates used in ring shear apparatus to maximise stress transfer into a clay material.

4 Results of 3D Printing Textured Geomembranes: Geotextile Interfaces

The first series of tests carried out were using geomembrane - geotextile interfaces. Samples were prepared using both FFF and SLS methods to firstly replicate a factory derived sample (the reference geomembrane), then secondly to investigate systematic changes in the geometric configuration of the geomembrane surface.

4.1 Comparison of Factory and Manufactured Texturing

Figure 4 presents the shear stress displacement curves of factory HDPE materials in comparison to those produced by FFF and SLS. At 50 kPa normal stress the SLS samples and factory materials follow a similar trend of shear behaviour with the SLS exhibiting a 4.5% higher peak value. At 200 kPa normal stress there is only 3% difference between the peak values, however, the factory material exhibits an earlier peak at around 6mm displacement, and less post peak shear strength loss is observed for the SLS material. At 400 kPa normal stress there is a more discernible difference of 12.3% as wear of the HDPE surface limits shear strength development (Zaharescu et al., 2015), but the PA SLS material is more resistant to this damage. A better correlation is observed between the rapid prototyped and reference geomembrane at lower normal stresses, but as the HDPE wear increases at higher normal stresses (Zaharescu et al., 2015), the trends diverge more noticeably, this is confirmed by comparison of the derived shear strength parameters summarised in Table 4 obtained from best fit straight lines through the measured peal values.

The relative performance of FFF samples to those manufactured using SLS is also given in Figure 4. The FFF samples exhibited 13.9 and 9.9% higher peak shear stress than the SLS samples at 50 and 200 kPa respectively, this generates the higher adhesion intercept shown in Table 4. This may be attributed to the print characteristics resulting in a rougher surface of the FFF samples, as discussed further in Section 7. At 400 kPa the results show a difference of only 0.3% between the peak values for the SLS and FFF samples.

Following the trials in Section 4.1 it was decided to proceed with SLS prototypes for the geometric variable analyses because of the better fit achieved with factory textures samples (Figure 4). To allow confidence in these analysis a series of repeatability tests were carried out on the SLS-GT interfaces, comprising three

additional tests at each normal stress. The results are presented in Figure 5 and summarised in Table 5, and demonstrate an average coefficient of variation of 2.6%. This is considered low when compared to repeatability testing by Sia and Dixon (2007), and may reflect the repeatable geometry, relative to the shear box boundaries, achieved using rapid prototyping.

4.2 Asperity Shape

The first investigation was to vary the asperity shape parameters comparing a standard spiked asperity to a hooked asperity. Hook and Loop interaction has been discussed by several authors, notably Hebeler et al. (2005) utilised optical microscopy to investigate the degree to which hook and loop interactions prevailed. However, due to the manufacturing process it has remained difficult to directly contract materials with and without hooks. Rapid prototyping allows a direct comparison of hooked and non-hooked asperities to directly assess the influence on interface shear strength. The nature of the shapes used are presented in Figure 3. Whilst more aggressive hooks have been trialled, the authors have selected those reported below to represent shapes more achievable in the geomembrane sprayed and co-extruded manufacturing processes.

The results from shear box testing are shown in Figure 6 and it is immediately apparent that the hooked asperities give significant increase in shear strength at low normal stresses. A 30.1 kPa increase in shear strength was observed at 50 kPa confining stress for hooked asperities. The influence of the hooks is reduced, in absolute and relative terms, at 200 kPa normal stress with the hooked asperities resulting in a 20.7 kPa increase in shear strength. At 400 kPa the hooks actually gave a slightly lower peak shear strength.

4.3 Altering Asperity Spacing

The next geometric variable to be investigated was the asperity density, i.e. the number of asperities on the sheet. The asperities were in lines, therefore, asperity density was altered by varying the spacing between asperities parallel to the shearing direction from a default of 10mm by ±3mm. Figure 7 shows the shear stress displacement curves for the three spacing arrangements and Table 4 summarises the shear strength parameters and also the number of asperities on the samples. Reducing the spacing to 7mm resulted in a 9.5%, 8.0% and 7.7% increase in peak shear strength at 50, 200 and 400 kPa respectively, compared to a reduction of 11.6%, 3.4% and 6.9 % respectively when increasing the spacing to 13mm.

4.4 Altering Asperity Height

281 The final geometric variable altered for the geomembrane was the asperity height. The expectation is that the
282 greater the asperity height, the greater the interlock at the interface between the geomembrane and
283 geotextile and the higher the peak shear stresses (Bacas, et al., 2015; Ivy, 2003; McCartney et al., 2005). The
284 standard height of 1mm was compared to the minimum GRI requirement of 0.4 mm (Geosynthetics Institute,
285 2016) (a reduction of 0.6mm) and 1.6mm (an increase of 0.6mm). The results of the analyses are shown in
286 Figure 8 and Table 4. Reducing the height from 1mm to 0.4mm, and proportionally scaling the dimensions of
287 the conical asperity resulted in a reduction in interface shear strength of 2.6%, 8.9% and 8.0% at 50, 200 and
288 400 kPa respectively. This contrasts with an increase in peak interface shear strength of 6.7%, 5.5% and 0.9%
289 respectively when the asperity height was increased to 1.6 mm. It should also be noted that the profiles
290 appeared much smoother with 0.4 mm asperities indicating more of a "stick - slip" interaction with the
291 geotextile obtained with the larger asperities.

292 **5 Results of 3D Printing Textured Geomembranes: Sand Interfaces**

293 As with the geotextile tests, a comparison was carried out between SLS manufactured and the reference HDPE
294 geomembrane. Figure 9 shows the shear stress displacement relationships for the geomembrane-sand
295 interfaces. At 50 kPa the reported shear stresses were very similar in the SLS manufactured and tests using the
296 reference HDPE geomembrane. At 200 and 400 kPa the SLS samples gave a higher strength by 10.0% and
297 11.1% respectively. Of particular note was the earlier (lower displacement) and higher peak at 400 kPa for the
298 SLS samples, and this correlates to the 16% lower magnitude and later (at greater shear displacement) dilation
299 for the HDPE samples shown in Figure 10.

300 **6 Results of 3D Printing Textured Geomembranes: Fine grained soil Interfaces**

301 As with the geotextile and sand tests, a comparison was carried out between SLS manufactured and the
302 reference HDPE geomembrane, which was followed by an investigation of the influence of the height and
303 spacing of asperity variables. An initial comparison between SLS manufactured and reference HDPE
304 geomembranes was carried out and the results are presented in Figure 11. The trends correlate well with a
305 difference of just 3.8%, 1.4% and 2.8% in the maximum observed shear stress at 50, 200 and 400 kPa confining
306 stresses respectively, for comparable 'spike' shaped asperities. Moreover, on observation of the samples the
307 HDPE geomembrane had observed negligible post shear wear, hence the polymer difference between the SLS
308 and HDPE has much less influence than in the geomembrane-sand tests reported in Section 5. It should be

noted that the shear stress presented in Figure 11 may not have reached full peak values within the displacement available using the small direct shear apparatus, therefore, the “peak” values discussed in this section and Section 6.1 refer to a maximum shear stress at or before maximum displacement was reached.

6.1 Spacing and Asperity Height

The SLS technique has been utilised in this study to investigate the influence of surface morphological variables on the interface shear strength at a geomembrane-clay interface. For the clay interface a series of ribs were selected as a simple geometric structure, similar to those adopted by McNamara *et al.* (2016) for increasing soil interaction on model piles. This configuration is commonly employed in standard direct shear devices to form high friction plates below and above the clay material being tested. The height of the ribs and the spacing were systematically varied as shown in Table 6, producing ten unique designs to be tested in a total of 90 shear box tests.

The peak strengths for the differing asperity spacings are shown in Figure 12. The repeatability of the testing procedure from each of 3 repeat tests are shown to be satisfactory with an average Coefficient of Variation of below 2% and a maximum of 6%. This can be attributed to the spatial repeatability of the geomembrane manufacture and also the careful control in preparation of the clay samples. This variability is comparable to that found by Sia and Dixon (2007) for a single operator and using the same materials in the same shear box. The results in Figure 12 suggest that there is a critical asperity spacing of 7-9mm, below and above which strength decreases by up to 15%. This decrease is observed despite an increase in the overall number of asperities with 11 bars present at 7mm spacing and 20 bars at 3mm spacing.

The influence of asperity height is shown in Figure 13. It might be anticipated that for higher asperities, greater shear strength would be measured. However, there was only a slight increase in shear strength as a result of increased asperity height with increases in peak shear stress of 3.9%, 2.7% and 4.2% at 50, 200 and 400 kPa respectively between the 0.4mm and the 2mm asperities.

7 Discussion

For the geomembrane-geotextile interfaces at normal stresses of 50 and 200 kPa, the results presented show that the correlation between the shear stress displacement curves for a factory HDPE material and the SLS samples are within the bounds of the natural variability of geosynthetic interfaces suggested by Sia and Dixon

(2007). Zaharescu et al. (2016) has shown geomembrane wear increases with normal stress, and at 400 kPa a 12.3% higher peak strength value was reported for the SLS sample than the factory HDPE, which is thought to be due to the stronger, stiffer PA SLS material underrepresenting the wear on the geomembrane. Whilst the FFF samples followed similar trends, the reported peak strengths were all more than 10% higher than for the factory HDPE material. This can be attributed to the FFF manufacturing process producing a second order roughness along the surface of the base sheet (the area between asperities) and along the asperities themselves. Further interrogation of the material surfaces is presented in Figure 14, which shows cross sections through the asperities derived from white light interferometry of the factory, SLS and FFF materials. The FFF material shows clear steps where one extruded layer meets another, which are less evident in the SLS materials adopted here. As a result of this, SLS techniques were preferred to FFF additive manufacturing in this study. However, it should be noted that these findings are a function of the equipment used in this investigation and is not simply an intrinsic function of the FFF and SLS techniques.

For the geomembrane-clay interfaces, the results presented show that the correlation between the shear stress displacement curves for a factory HDPE material and the SLS samples are within the bounds of the natural variability of geosynthetic interfaces suggested by Sia and Dixon (2007). This was also the case for the geomembrane-sand interfaces at 50 kPa normal stress, however, at 200 and 400 kPa normal stresses the stiffer, stronger PA SLS samples reported a 10.0 and 11.1% higher peak shear stress respectively. Visual inspection of the sheared surfaces indicates that the sand causes greater wear to the surface of the factory HDPE geomembranes, whereas the factory HDPE geomembranes sheared against clay did not experience morphological changes. This investigation indicates that the correlation between the factory HDPE and SLS geomembranes are better in scenarios where the “wear” on the geomembrane surface is low. Whereas, for the higher wear geomembrane-sand interfaces, the correlation is less satisfactory, due to the more resistant PA polymer. The geomembrane-soil correlations are in agreement with the geomembrane-geotextile interfaces, where the HDPE geomembranes suffer less wear at lower normal stresses, as indicated by Frost et al., (2002) and Zaharescu et al., (2015).

The subtractive techniques tested in this study were not effective at reproducing the texturing found on the reference material. Such techniques are better suited to cutting through the full thickness of a sheet, for example when prototyping geogrids. Subtractive manufacture offers the desirable advantage of utilising the

same polymeric materials and pre subtraction manufacturing as a factory geomembrane, therefore, these techniques warrant further investigation in future.

When considering the influence of asperity shape variables on the interface performance, hooks were found to increase the peak strength of the interface by 69% at 50 kPa normal stress as a result of better macroscale interaction with the fibrous geotextile, as suggested by Hebeler et al. (2005). The influence of the hooks is less prevalent at 200 kPa normal stress, however it still resulted in an 18% strength increase. At 400 kPa the hooks actually gave a slightly lower peak shear strength, this may be attributed to the hooks being more susceptible to damage than the more stable conical asperities, and indeed on further inspection the samples showed some hooks experienced damage to the peak of the asperities.

Closer spacing of asperities resulted in higher recorded peak strengths for the geomembrane-geotextile interfaces, as the greater number of asperities allowed distribution of the shear stress across a larger number of fibres within the geotextile. However, for the geomembrane clay interfaces, an optimum spacing of 7-9 mm was recorded. As spacing reduced beneath this range, a failure plane was seen to develop across the top of the asperities as indicated in Figure 15. This demonstrates the importance of maintaining sufficient inter-asperity soil friction as described by Bacas et al. (2015) rather than simply assuming greater asperity distribution is proportional to shear strength. This optimum spacing reported may be both soil and polymer specific, however, this study provides a valuable insight into the soil – texture interaction, and rapid prototyping allows researchers and manufactures to assess the influence of such variables without costly production modifications.

For the geomembrane-geotextile interfaces, sample height was found to give a 2.6-8.9% increase in peak strength from 0.4 mm to 1.0 mm asperity height, but negligible benefits were reported when increasing height from 1.0 mm to 1.6mm. The smoother recorded shear stress displacement with 0.4 mm asperities compared to the “stick - slip” recorded with 1.0 mm and 1.6 mm asperities is possibly due to the greater embedment depth, with the greater heights resulting in more fibres interacting with each asperity. For the geomembrane-clay interfaces, there was a maximum 4.2% difference in peak stress recorded between the 0.4mm and 2mm high asperities, this implies that 0.4mm is adequate to transfer the shear stress and is still very large compared to the grain size of the soil material being tested. It should be noted that these interfaces were not

391 "submerged", and further work is required to assess if greater asperity height influences results if free fluid is
392 available at the interfaces.

393 Whilst the SLS technique allowed systematic investigation of geometric variables, consideration in the findings
394 must always be given to the analogy between the modelled material and a factory HDPE geomembrane. An
395 example is the influence of hooks discussed in Section 4.2, which shows there are significant benefits
396 especially at 50 kPa normal stress, however, a hook formed from flat die extruded HDPE may or may not be
397 able to withstand the same localised stress concentration as in the SLS material. Despite this limitation, it
398 demonstrates which asperity variables are worthy of greater consideration in the development process, and
399 allows a screening of the variables that have potential to improve interface strength. Moreover, the
400 application of rapid prototyping is not limited simply to the development of texturing, but could be used across
401 the geosynthetics industry from the investigation of soil-geogrid interaction, to optimising fluid flow in
402 drainage cores.

403 The studies reported in this investigation utilised a modified 100 mm x 100 mm shear apparatus. Therefore,
404 the study has focused on peak shear strength achieved, as the limited displacement of 19 mm does not allow
405 meaningful assessment of post peak behaviour. Moreover, it is acknowledged that the absolute results from a
406 larger DSA with floating upper top assembly may more accurately characterise interface behaviour
407 (Stoewahse, et al., 2002; Swan, 2004; Bemben and Schulze, 1998) and, therefore, tests are being undertaken
408 to investigate the viability of testing 305 x 305 mm printed geomembranes.

409 **8 Conclusions**

410 Rapid prototyping offers a platform technology for investigations within the geosynthetics research and
411 manufacturing sectors. Current rapid manufacturing techniques offer the ability to test the influence of
412 variables on the performance characteristics of geosynthetic materials. The limitations of each technique must
413 be understood to allow these techniques to be successfully deployed. From the study presented herein the
414 following conclusions can be drawn.

415 Additive manufacturing techniques can produce prototype model samples that represent the interface
416 behaviour of textured geomembranes with sufficient accuracy to be beneficial to the further scientific
417 investigation of texturing geometries. The correlation between manufactured and factory HDPE

418 geomembranes is better for scenarios where geomembrane surface wear is low, including geomembrane-clay
419 interfaces, and geomembrane-geotextile interfaces at low normal stresses.

420 Of the techniques trialled, additive manufacturing using selective laser sintering has shown the best
421 correlations with factory reference geomembrane, likely due to the high spatial resolution achievable and
422 better interlayer bonding. The internal extruded structure of fused filament fabrication samples was more
423 pronounced, resulting in a rougher surface and higher shear stress development. Subtractive manufacture
424 techniques were less successful in this study, however, have benefits of polymer type and internal structure.

425 For geomembrane-geotextile interfaces, the introduction of hooks to the asperities was effective at increasing
426 shear strength substantially (69%) at low (50kPa) normal stresses, but resulted in little benefits at higher (400
427 kPa) normal stresses. Increasing asperity spacing was shown to decrease peak shear strength for
428 geomembrane-geotextile interfaces but closer spacing increased interface strength. For geomembrane-clay
429 interfaces an optimum spacing of ribs was found at 7 to 9mm, with closer spaced asperities resulting in an
430 over-sliding mechanism and a reduction in strength. Increases in asperity height correlated to smaller than
431 expected increases in shear stresses for geomembrane-geotextile interfaces. For geomembrane-clay interfaces
432 asperities of 0.4 mm were found to be adequate to transfer stress to the soil in unsubmerged conditions.

433 **Acknowledgement**

434 The support provided by Loughborough University the Engineering and Physical Sciences Research Council
435 (EPSRC) through grant EP/M015483/1 is gratefully acknowledged. The Authors also wish to thank the IGS UK
436 Chapter for project funding and Golder Associates (UK) Ltd, Coffey Geotechnics Ltd and AECOM for in kind and
437 technical support.

438 **ABBREVIATIONS**

439 FFF Fused filament Fabrication

440 HDPE High Density Polyethylene

441 LBS Leighton Buzzard Sand

442 LTA Laser Thermal Ablation

443 (X)MD (Cross) Machine Direction

444 MM Mercia Mudstone

445 PA Polyamide

446 PP Polypropylene

447 SLS Selective Laser Sintering

448 **REFERENCES**

449 Bergado, D. T., Ramana, G. V., Sia, H. I.,Varun., 2006. Evaluation of interface shear strength of composite liner
450 system and stability analysis for a landfill lining system in Thailand. Geotex. and Geomembr., 24 (6), 371-393.

451 Bacas, B. M., Cañizal, J., Konietzky, H., 2015. Frictional behaviour of three critical geosynthetic interfaces.
452 Geosynth. Int., 22, No. 5, 355–365.

453 Baechler, C., DeVuono, M., Pearce, J.M., 2013. Distributed recycling of waste polymer into RepRap feedstock,
454 Rapid Prototyping Journal, Vol. 19 Iss 2 pp. 118 – 125

455 Bemben, S. M., Schulze, D. A., 1998. The influence of equipment style and setup dimensions on
456 sand/geomembrane direct shear test measurements. In: Rowe, R. K. (Ed.), Proc. of 6th Int. Conf. on Geosynth.,
457 Atlanta, Georgia, USA, 25-29 March, pp. 453-458.

458 Dixon, N., Jones, D. R. V., Fowmes, G. J., 2006. Interface shear strength variability and its use in reliability-
459 based landfill stability analysis. Geosynth. Int., 13. No. 1, 1–14.

460 Dove, J.E., Frost, J.D., 1996. A Method for Measuring Geomembrane Surface Roughness. Geosynth. Int., 1996,
461 Vol 3, No. 3. 369 – 392.

462 Dove, J., Frost, J., 1999. Peak Friction Behaviour of Smooth Geomembrane-Particle Interfaces. J. Geotech. and
463 Geoenviron. Eng., 125(7), 544-555.

464 Filz, G. M., Esterhuizen, J. J. B., Duncan, J. M., 2001. Progressive failure of lined waste impoundments. J.
465 Geotech. and Geoenviron. Eng., 127 (10), 841-848.

Fowmes, G.J. Dixon, N. Zaharescu, A., Fu, L., 2016. 3D Printing of High Strength Geosynthetic Interfaces. Proc. GeoAmericas, April 2016, Miami.

Frost, G. JD; Evans TM; Hebeler,G.L., Giroud, J., 2002. Influence of wear mechanisms on geosynthetic interface strengths. In GEOSYNTHETICS: State of the art-recent developments. Proc. 7th Int. Conf. on Geosynth., Nice, France. Volume 4.

Geosynthetics Institute, 2016. Test Methods, Test Properties and Testing Frequency for High Density Polyethylene (HDPE) Smooth and Textured Geomembranes, GRI Test Method GM13. Revision 14: January 6, 2016. Geosynthetic Institute, 475 Kedron Avenue Folsom, PA, USA

Gibson, I., Shi, D., 1997. Material Properties and Fabrication Parameters in Selective Laser Sintering Process. Rapid Prototyping Journal, 3(4), 129-136.

Godley, M., Zaharescu, C.A., Fowmes, G.J., 2015. Effect of Shear Rates on Geotextile - Geomembrane Interfaces. Geosynthetics 2015, Portland, Oregon.

Goodridge, R., Tuck, C., Hague, R, 2012. Laser Sintering of Polyamides and other Polymers. Progress in Materials Science, 57(1), 229-267.

Hebeler, G., Frost, J., Myers, A, 2005. Quantifying hook and loop interaction in textured geomembrane-geotextile systems. Geotext. and Geomembr. 23 (1), 77–105

Ivy, N., 2003. Asperity height variability and effects. GFR, 21, October–November, 28–29.

Jing, Xue-Ying, Wan-Huan Zhou, Yangmin Li., 2017. Interface direct shearing behaviour between soil and saw-tooth surfaces by DEM simulation. Procedia Engineering 175 (2017): 36-42

Jollivet, T., Darfeuille, A., Verquin, B., Pillot, S., 2009. Rapid Manufacturing of Polymer Parts by Selective Laser Sintering. Int. J. Material Forming, 2(1), 697-700.

Jones, D.R.V., Dixon, N., 2003. Stability of Landfill Lining Systems: Literature Review, Bristol: Environment Agency Research and Development Project, pp.1-385.

Koerner, R. M., Bowman, H. L., 2003. A recommendation to use peak shear strengths for geosynthetic interface design. Geotechnical Fabrics Report, April 2003.

Kruth, J. 1991. Material Increase Manufacturing by Rapid Prototyping Techniques. Annals of the CIRP, 40(2), 603-614.

Kruth, J., Wang, X., Laoui, T., Froyen, L., 2003. Lasers and Materials in Selective Laser Sintering. Assembly Automation, 23(4), 357-371.

Koerner, R., Soong, T., 2000. Stability Assessment of Ten Large Landfill Failures. In: Proceedings of GeoDenver2000: Advances in Transportation and Geoenvironmental Systems using Geosynthetics, Denver, Colorado, 5th-8th August 2000, New York: ASCE, pp. 1-38.

Koerner, G.R., Narejo, D., 2005. Direct shear database of geosynthetic - geosynthetic and geosynthetic-to-soil interfaces. GRI Report #30, Geosynthetic Research Institute, USA.

Lupo, J., 2010. Liner System Design for Heap Leach Pads. Geotex. and Geomembr., 28(2), pp. 163-173.

McNamara, A. M., Gorasia, R.J., 2016. High-capacity ribbed pile foundations. Proc. of the Institution of Civil Engineers: Geotech. Eng., 169(3), pp. 264-275.

McCartney, J. S., Zornberg, J. G., Swan, R. H., 2005. Effect of geomembrane texturing on GCL–geomembrane interface shear strength. In Waste Containment and Remediation. GeoFrontiers, 2005.

McCartney, J., Zornberg, J., Swan, R., 2009. Analysis of a Large Database of GCL-Geomembrane Interface Shear Strength Results. Journal of Geotechnical and Geoenvironmental Engineering, 135(2), 209-223.

Schmid, M., Amado, A., Wegener, K., 2014. Materials Perspective of Polymers for Additive Manufacturing with Selective Laser Sintering. J. Materials Research, 29(17), 1824-1832.

Sia, A.H.I., Dixon, N., 2007. Distribution and variability of interface shear strength and derived parameters. Geotex. and Geomembr., 25(3), pp.139–154.

511 Stark, T. D., Williamson, T. A., Eid, H. T., 1996. HDPE geomembrane/geotextile interface shear strength. J.
512 Geotech. Eng., ASCE, 122 (3), 197-203.

513 Stathas, D., Wang, J.P., Ling, H.I., 2017. Model geogrids and 3D printing, Geotex. and Geomembr. 2017.
514 http://dx.doi.org/10.1016/j.geotexmem.2017.07.006

515 Stoewahse, C., Dixon, N., Jones, D. R. V., Blumel, W., Kamusgisha, P., 2002. Geosynthetics interface shear
516 behaviour: Part 1 test methods. Ground Eng., 35 (2), 35-41.

517 Swan, R. H., Jr. 2004. The importance of interface shear strength and the major factors, which can influence
518 the measured shear strength results. Geotechnical Fabrics Report. 2004.

519 Tan, S. A., Chew, S. H., Wong, W. K., 1998. Sand-geotextile interface shear strength by torsional ring shear
520 tests. Geotex. and Geomembr., 16 (3), 161-174.

521 Thiel, R. S., 2001. Peak vs. residual shear strength for landfill bottom liner stability analyses. In: Proceedings of
522 15th Geosynthetic Research Institute Conference on Hot Topics in Geosynthetics-II, Folsom, Pa.: GRI
523 Publishers, pp. 40-70.

524 Triplett, E. J., Fox, P. J., 2001. Shear strength of HDPE geomembrane/ geosynthetic clay liner interfaces. J.
525 Geotech. and Geoenv. Eng., 127, No. 6, 543–552

526 Vangla, P., Latha, G. M., 2016. Surface topographical analysis of geomembranes and sands using a 3D optical
527 profilometer. Geosynth. Int. 24 (2), 151-166.

528 Zaharescu, C.A. Fowmes, G. J. Dixon N., Wu, H., 2015. Geosynthetic-Geosynthetic Interface Behaviour Analysis
529 Using Digital Imaging. Proc. Geosynthetics 2015, Portland, Oregon.

530 Zettler, T., Frost, J., DeJong, J., 2000. Shear Induced Changes in Smooth HDPE Geomembrane Surface
531 Topography. Geosynth. Int., 7(3), 243-267.

532 **List of Tables**

540

541 Table 1. Summary of Geotextile properties

Property	Standard	Value
Static puncture strength	BS EN ISO 12236	14 kN
Push-through displacement	BS EN ISO 12236	65 mm
Tensile strength	BS EN ISO 10319	75 kN/m
Thickness @2kPa		7.8 mm

548

549 Table 2. Summary of Reference Geomembrane properties

Property	**Value**
Polymer	HDPE
Sheet thickness	1.5 mm
Asperity Height	1.0mm
Texture Type	Roller applied structured spike pattern
Distance between Asperities (MD/XMD)	10.0mm/10.0mm
Asperity Base Diameter	1.5mm
Density	0.942 g/cm^3

560

561 Table 3. Material properties for the Mercia Mudstone

Properties	**Value**
Specific Gravity, Gs (Mg/m^3), (BS 1377-2:1990)	2.77
Atterberg Limits, (BS 1377-2:1990**)**	
Liquid Limit, w_L (%)	34.1
Plastic Limit, w_P (%)	17.3
Plasticity Index, PI (%)	16.8
Compaction (BS 1377-4:1990)	
Optimum moisture content, OMC (%)	12.7
Maximum dry density, $\rho_{dry,max}$ (Mg/m^3),	1.96
Grain Size Analysis, (BS EN ISO 14688-1:2013 **)**	
D60 (mm)	0.26
D30 (mm)	0.11
D10 (mm)	0.003
Cu (uniformity coefficient)	86.7
Cc (curvature coefficient)	0.16

562

563 Table 4. Comparison of Factory HDPE and Selective Laser Sintering and Fused Filament Fabrication Texturing

564 peak shear strength parameters

	Shape	Asperity Height (mm)	MD Spacing (mm)	Asperities on sample (No.)	Adhesion (kPa)	Friction Angle (°)
Factory HDPE	Spike	**1.0**	**10**	**116**	20.7	24.2
SLS (copy of Factory HDPE)	Spike	1.0	10	116	15.3	27.8
FFF (copy of Factory HDPE)	Spike	1.0	10	116	25.6	26.8
SLS Hooked	Hook	1.0	10	116	56.8	21.4
SLS 7mm Spacing	Spike	1.0	**7**	**160**	22.3	27.4
SLS 13mm Spacing	Spike	1.0	**13**	**83**	13.8	26.4
SLS 0.4 mm Height	Spike	**0.4**	10	116	15.9	25.6
SLS 1.6 mm Height	Spike	**1.6**	10	116	19.8	27.7

565

566 Table 5. Repeatability of Selective Laser Sintered GM – GT Tests

Normal Stress	SLS Sample	Repeat 1	Repeat 2	Repeat 3	Standard Deviation	Mean	Coefficient of Variation
(kPa)	Maximum Shear Stress (kPa)				(kPa)	(kPa)	%
50	44.82	45.06	47.01	47.42	1.32	46.08	2.88
200	115.21	118.04	118.09	114.02	2.05	116.34	1.76
400	228.67	215.58	231.15	223.34	6.89	224.69	3.07

567

568

569

570 Table 6. Programme of SLS manufactured Geomembrane vs Clay Direct Shear Apparatus Tests

Normal Stress (kPa)	Material ID	Bar height (mm)	Bar spacing (mm)	Number of test repetitions
50,200 & 400	FB1	1.0	3	3
	FB 2	1.0	5	3
	FB 3	1.0	7	3
	FB 4	1.0	9	3
	FB 5	1.0	11	3
	FB 6	1.0	13	3
	FB 7	1.0	15	3
	FB 8	0.4	7	3
	FB 9	1.5	7	3
	FB 10	2.0	7	3

571

572 **List of Figures**

591

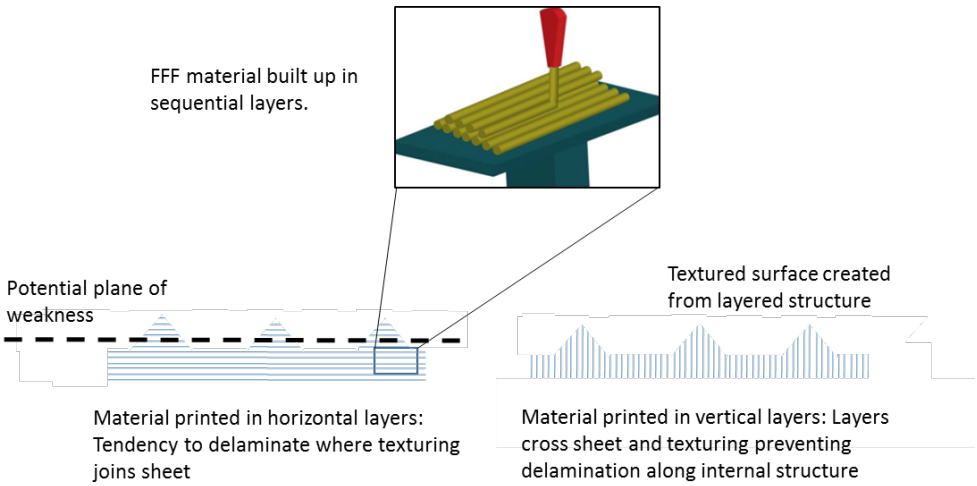

592

593 Figure 1. Printing of geosynthetics in layers parallel to the sheet and perpendicular to the sheet (after Fowmes

594 et al., 2016)

595

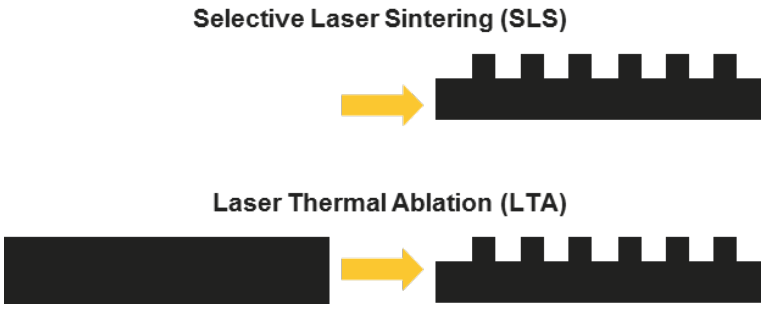

596

597 Figure 2. Comparison of ‘additive’ SLS process and ‘subtractive’ LTA manufacturing

598

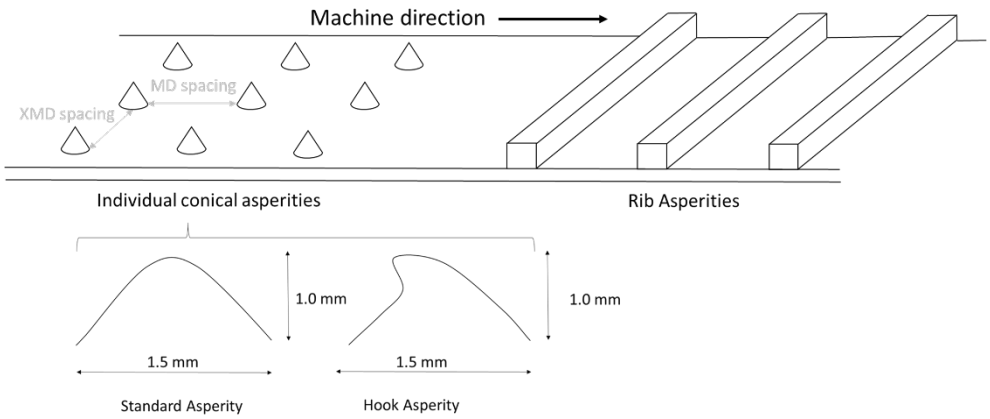

599

600 Figure 3. Schematic and cross section through asperity shapes

601

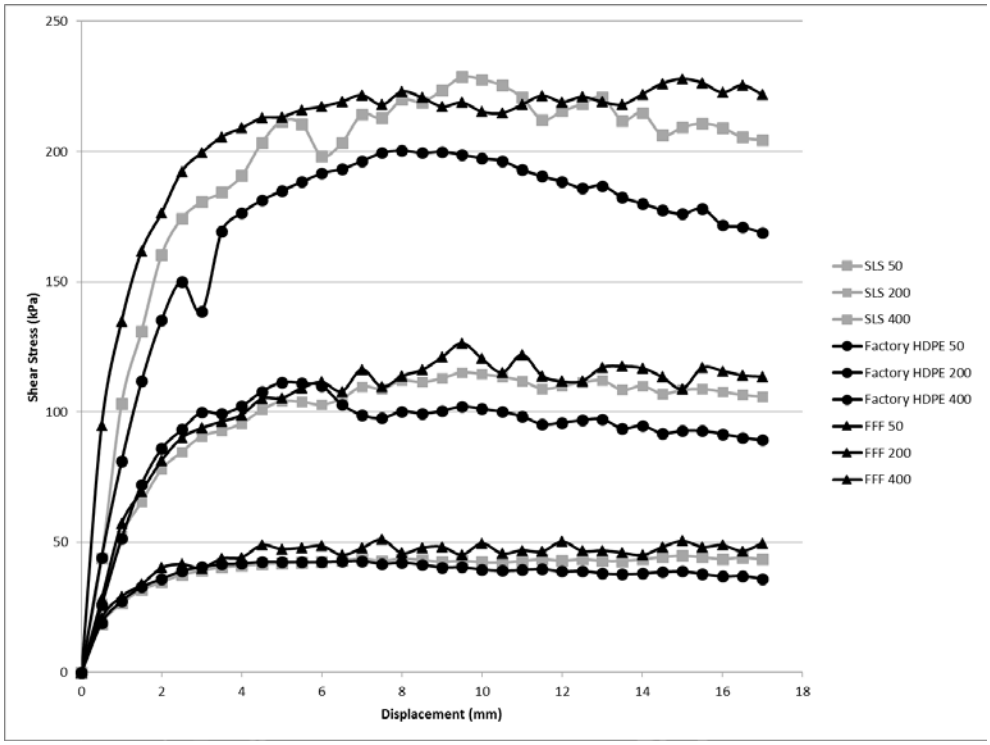

602

603 Figure 4. Comparison of factory HDPE, fused filament fabrication and laser sintering for GM-GT interface.

604

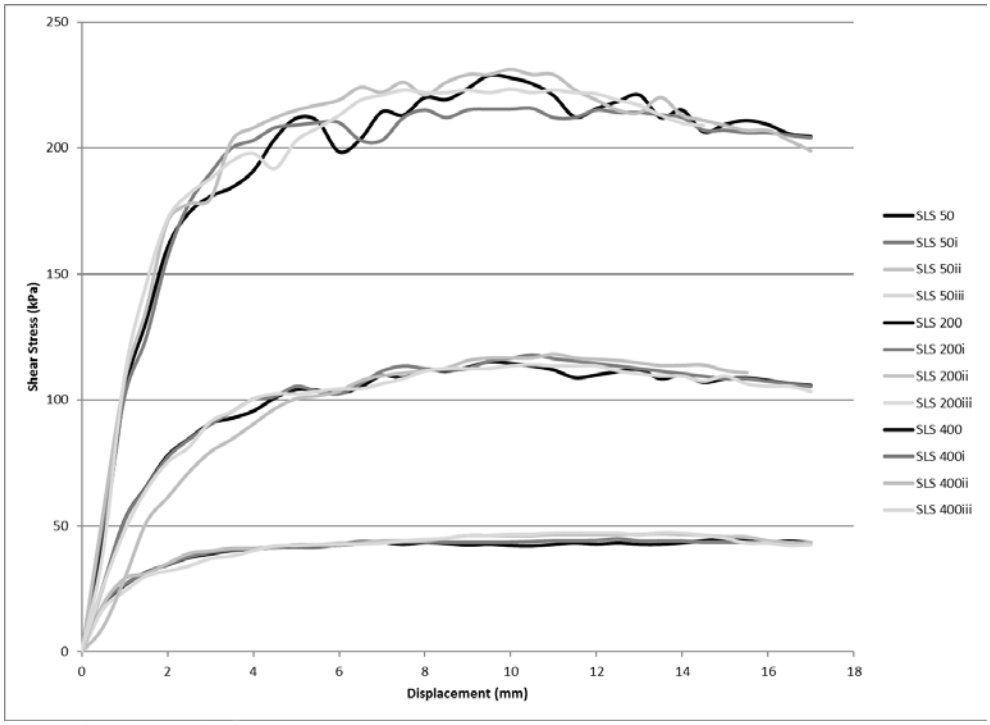

605

606 Figure 5. Repeatability test results for laser sintered GM-GT interface

607

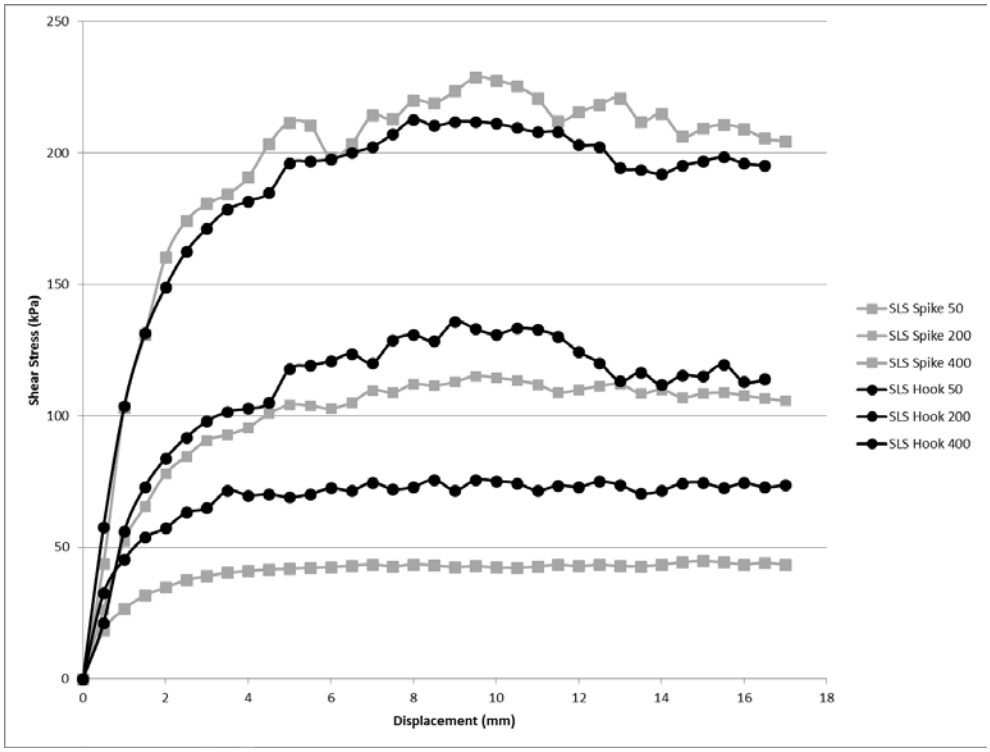

608 Figure 6. Results showing influence of altering asperity shape on a geomembrane-geotextile interface

609

610

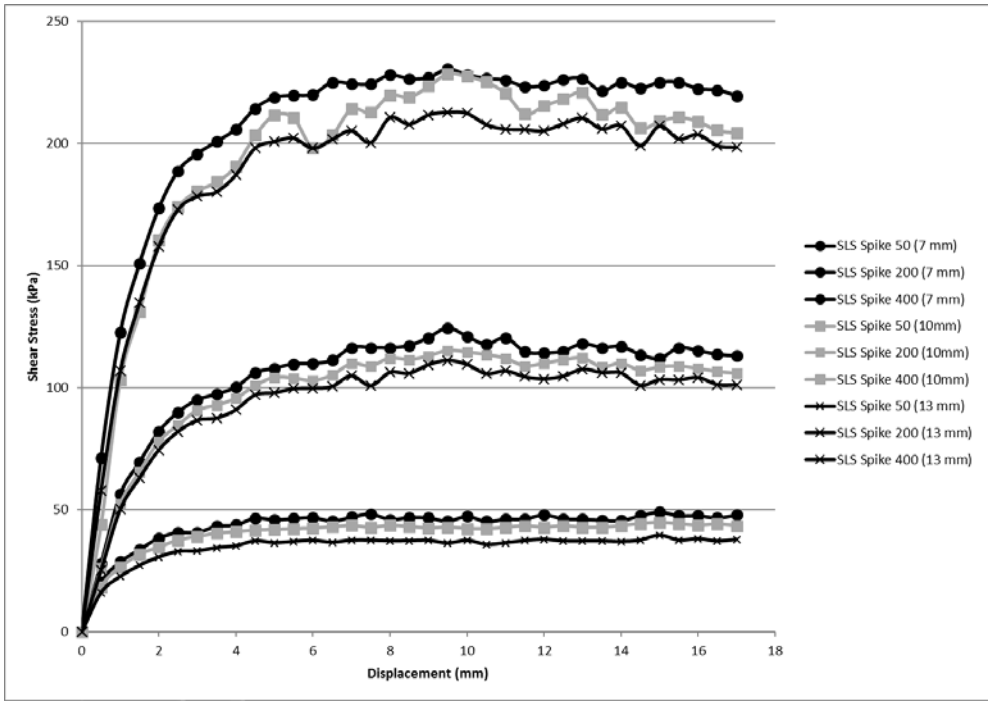

611 Figure 7. Results showing influence of altering asperity spacing on a geomembrane-geotextile interface

612

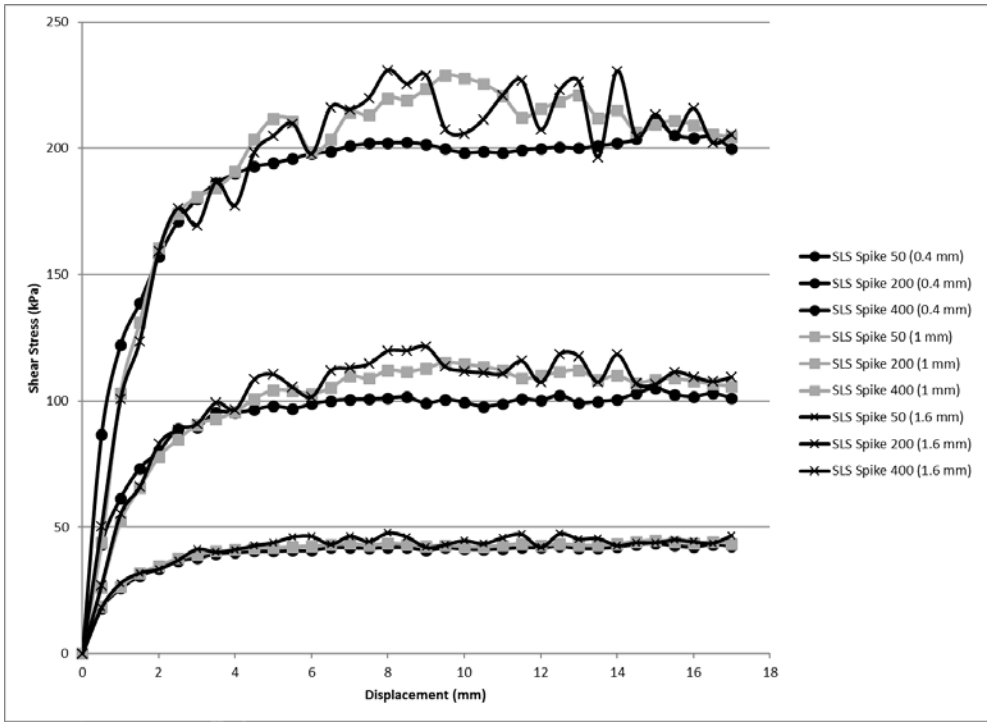

613

614 Figure 8. Results showing influence of altering asperity height on a geomembrane-geotextile interface

615

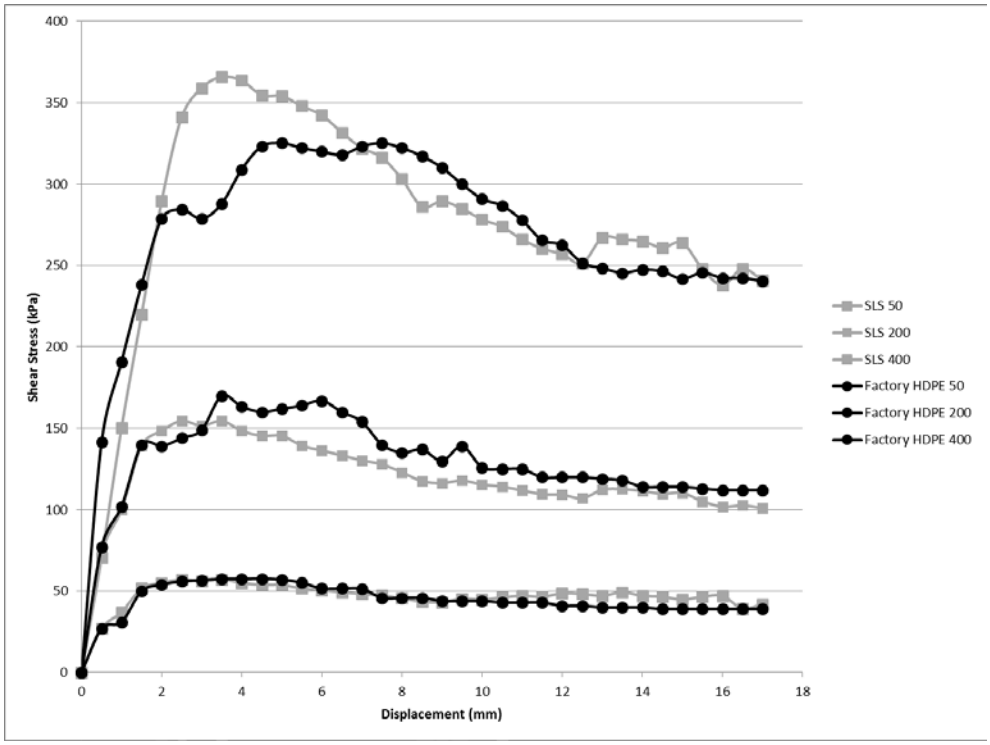

Figure 9. Comparison of factory HDPE and Laser Sintering for GM-Sand Interface

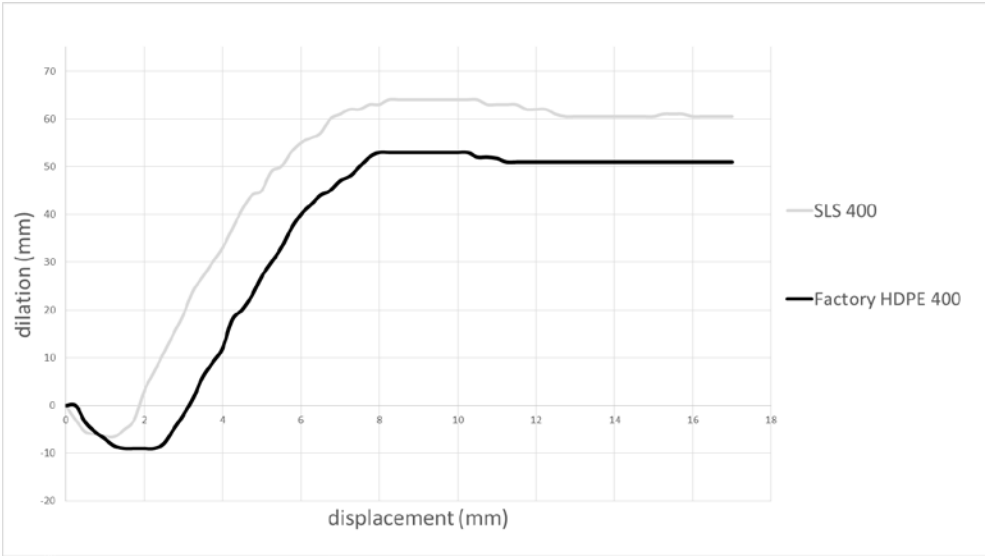

619

620 Figure 10. Comparison of dilation for factory HDPE and Laser Sintering for GM-Sand Interface

621

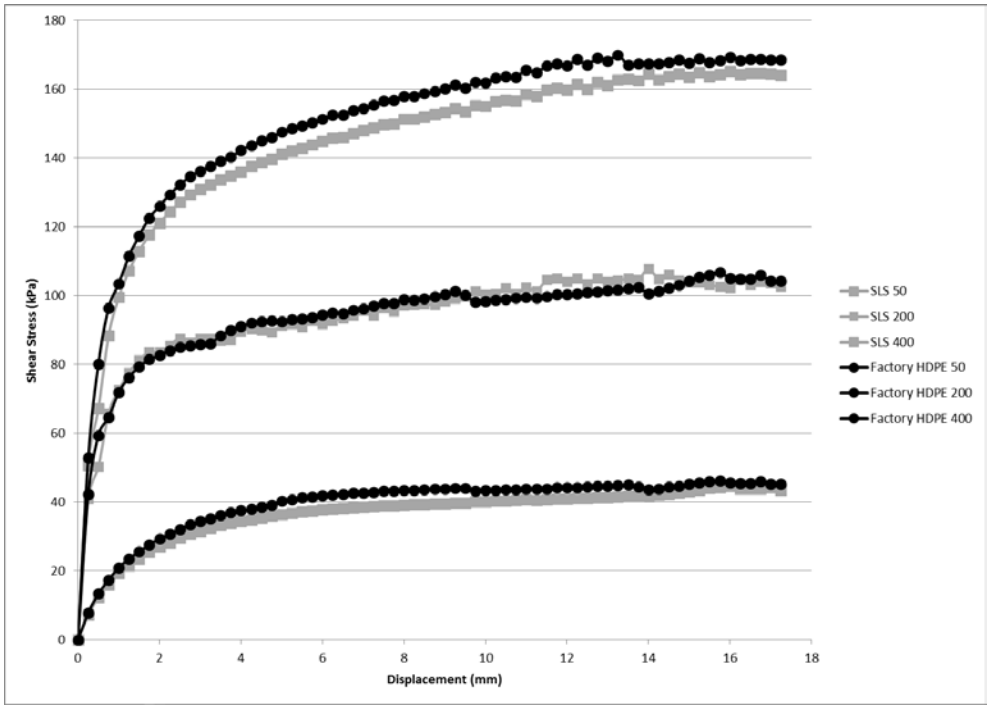

622

623 Figure 11. Comparison of factory HDPE and Laser Sintering for GM-Clay Interface

624

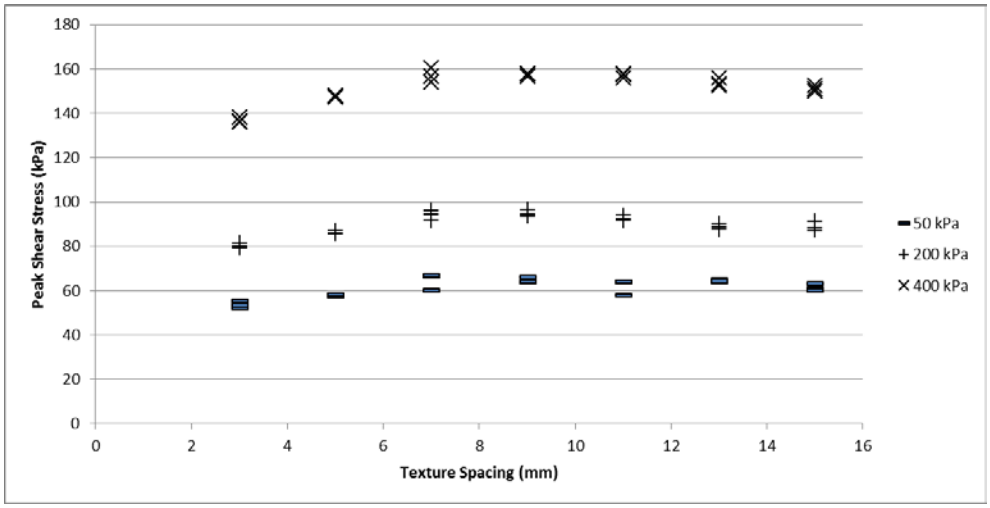

Figure 12. Influence of geomembrane asperity spacing for GM-Clay interfaces (each marker represents peak shear stress at one of the three repeat tests at each spacing and normal stress)

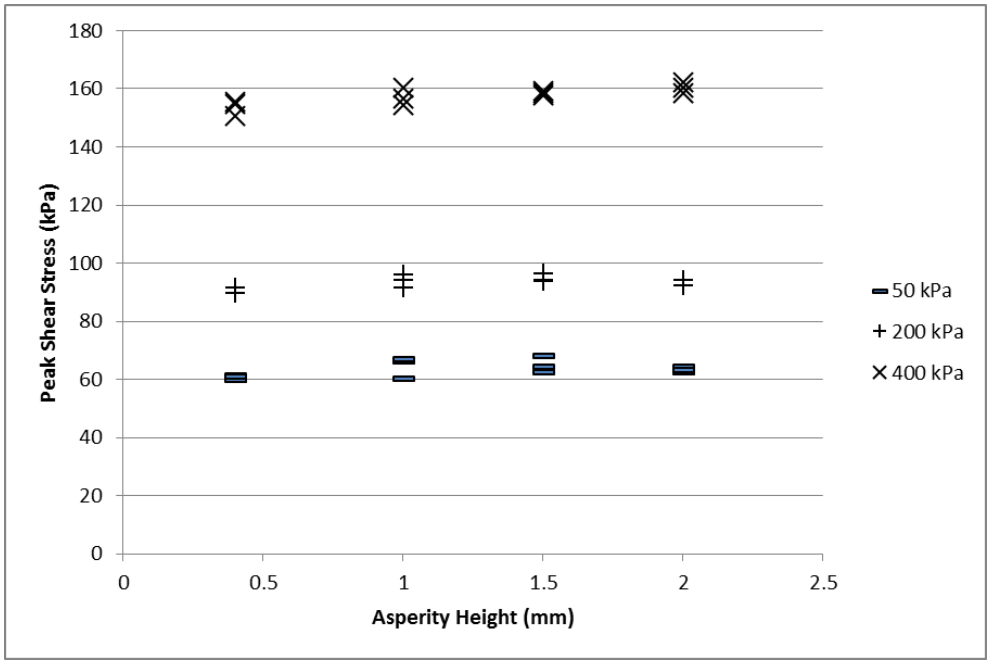

629

630 Figure 13. Influence of geomembrane asperity height for GM-Clay interface (each marker represents peak

631 shear stress at one of the three repeat tests at each spacing and normal stress)

632

633 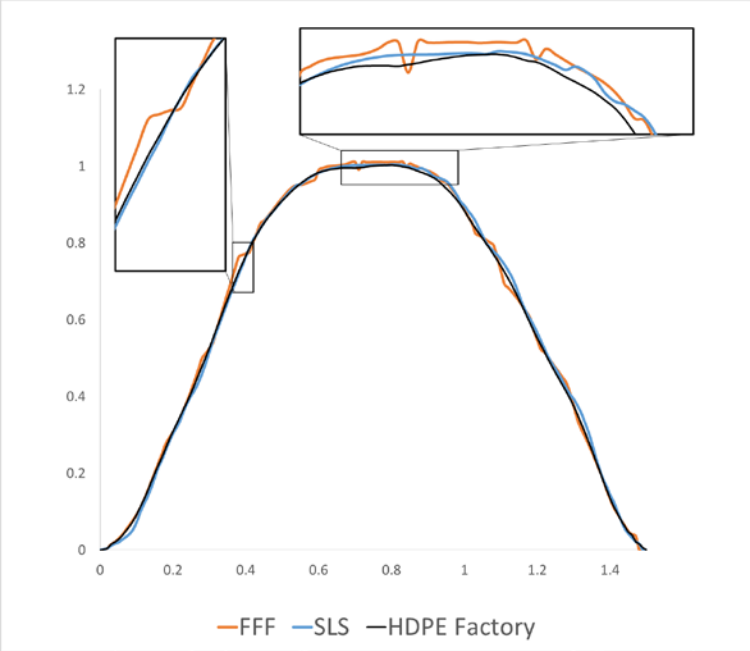

634 Figure 14. Interferometry comparison of pre-sheared factory HDPE and additive manufactured samples

635

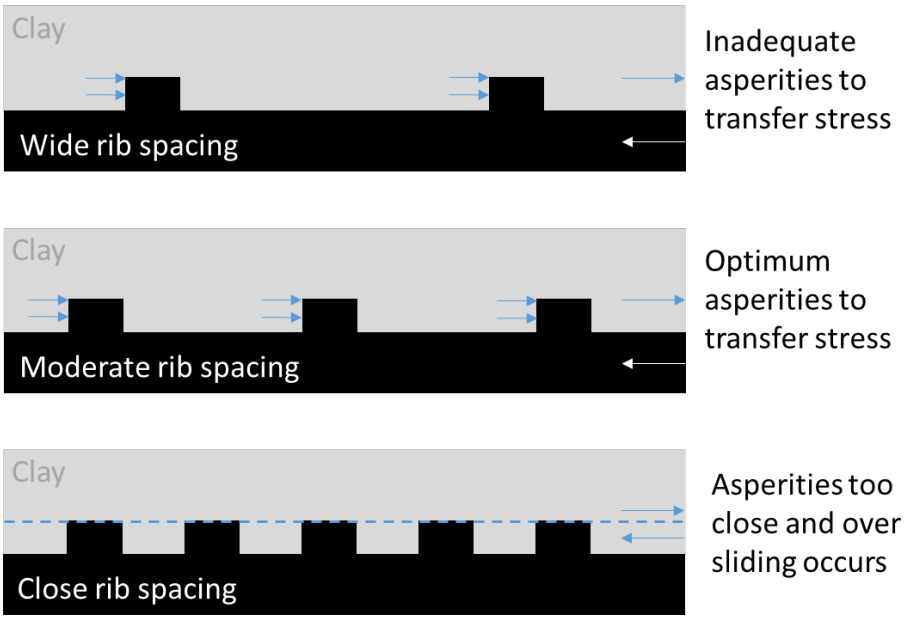

636

637 Figure 15. Schematic showing the optimum asperity spacing for geomembrane-clay interfaces

638